A validated methodology for patient specific computational modeling of self-expandable transcatheter aortic valve implantation

Title: A validated methodology for patient specific computational modeling of self-expandable transcatheter aortic valve implantation

Authors:

Bart Bosmans[1,2,3], Nele Famaey[1], Eva Verhoelst[2], Johan Bosmans[3], Jos Vander Sloten[1]

Affiliations:

[1] KULeuven, Faculty of Engineering Science, Celestijnenlaan 300C, 3001 Leuven, Belgium. Department of Mechanical Engineering, Biomechanics Section

[2] Materialise N.V., Technologielaan 15, 3001 Leuven, Belgium

[3] University of Antwerp, Faculty of Medicine and Health Sciences, Universiteitsplein 1, 2610 Antwerp, Belgium. Department of Translational Pathophysiological Research, Cardiovascular diseases

Met opmaak: Engels (V.S.)

Met opmaak: Engels (V.S.)

Word count (introduction through discussion, 3500): 3484

Corresponding author:

Bart Bosmans

KULeuven – Departement of Mechanical Engineering, Biomechanics Section

Technologielaan 15,

3001, Leuven, Belgium.

Tel: +32 16 396 728

Fax: +32 16 396 606

Bart.Bosmans@kuleuven.be

Abstract (250 words)

Voor mij wat rommelig

Meestal breng je in een abstract duidelijk aan wat background, onderzoeksvraag, gebruikte methode, resultaten (en dan wat meer "quantitatief" en besluit zijn

Leakage of blood (paravalvular aortic regurgitation) alongside the implant is a relatively frequent and life-limiting complication after transcatheter aortic valve implantation. The aim of this study is to develop and validate a workflow to simulate the implantation prior to the intervention. Based on the simulation outcome, an estimation of the amount of leakage is made in order to estimate the risk of acquiring this complication. A finite element model of the stent implantation in 10 patients was created based on a pre-operative computed tomography scan. All 10 patients also received a follow-up computed tomography scan, after the implantation. This scan was used to extract the deformed geometry of the stent and the position of the calcifications for validation of the simulation results. The maximal average cross sectional difference between the simulated stent and the post-operative stent is 1.1 mm, and occurs at the bottom of the device. The sensitivity of the simulation to the soft tissue material parameters and aortic root wall thickness was tested. The maximal diameter deviation of 6% occurred when the thickness of the aortic root was doubled. The result of the leakage analysis based on the distance between the simulated stent and the surrounding aortic root corresponded well when no regurgitation was observed. The developed tools have the potential to reduce the occurrence and severity of leakage by providing the clinician with additional information prior to the intervention. The simulated geometry and estimated leakage can help decide on the best implant type, size and position before treatment.

Met opmaak: Nederlands (België)

Met opmaak: Nederlands (België)

Met opmaak: Nederlands (België)

Introduction

Aortic valve stenosis is the most commonly acquired valvular heart disease in the elderly. Despite advances in cardiac surgery and low mortality rates after conventional surgical aortic valve replacement, up to one third of patients with symptomatic aortic valve stenosis are not considered for valve replacement, often due to age, frailty or co-morbidities [Bose et al., 2007; Thourani et al., 2011]. Transcatheter aortic valve implantation (TAVI) has been proven to be a reasonable alternative for the treatment of aortic valve stenosis in elderly (very) high-risk patients [Kodali et al., 2012]. However, aortic regurgitation (AR) after TAVI remains a frequent and life-limiting complication [Leon et al., 2010; Linke et al., 2014]. Leakage alongside the implant, paravalvular AR, is hypothesized to originate from the interaction between the implant and the calcified native aortic root. In contrast to conventional surgery, the calcifications and leaflets are not removed during a TAVI procedure. The anchoring of the device is dependent on the calcifications.

Due to the complex physical interactions of the different materials and geometries, computational modeling is the best approach to evaluate and predict the deployment process during a TAVI intervention. With appropriate validation, these models could be used to aid the clinical decision and planning process of the TAVI intervention. In recent literature, there are some studies which investigate and report finite element simulation of this intervention [Auricchio et al., 2014; Bailey et al., 2015; Capelli et al., 2012; Morganti et al., 2014; Russ et al., 2013; Wang et al., 2012]. However, to the best of our knowledge, only Russ et al. (2013) compare their result with a post-operative scan to verify the accuracy of their simulation result. Therefore, the goal of this paper is to develop a simulation workflow based on pre-operative clinically available data, which allows to predict the post-operative geometry and estimate the paravalvular AR, and validate it with post-operative scans and aortic regurgitation evaluation of treated patients.

Material and methods

10 patients received a contrast enhanced, ECG-triggered, end diastolic computed tomography (CT) scan both before and at a follow-up after the TAVI procedure. The scans were performed on a 64-slice GE lightspeed (General Electric Company, Easton Turnpike, Fairfield, CT, USA) with a spatial resolution of 0.6 mm. All patients received an intravenous injection of 80ml of contrast agent at a flow rate of 4 ml/s, followed by 30 ml at 2.5 ml/s.

De paragraaf die nu komt bevat ook al resultaten, wat verwarrend is in deze methode paragraaf. The average age of the patients was 74.2 years, three patients were female. All received a 29 mm CoreValve implant (Medtronic Inc., Minneapolis, MN, USA). The minimum volume of calcification, measured as the internal volume of the segmented surface, is 17 mm^3, the maximum volume is 482 mm^3 and the median volume is 57 mm^3, indicating a skewed distribution over the 10 patients. AR was graded at two separate points in time: (1) immediately after the implantation on the procedural angiography, as described by Seller *et al.* [Sellers et al., 1964], and (2) at hospital discharge or within 7 days after the implantation procedure using transthoracic echocardiography as described by Collas *et al.* (2015). Column 3 and column 4 of table 7 contains the results of these measurements. At both times only, one out of the 10 patients in this study had an AR grade greater than or equal to 2, which is considered a predictor of higher mortality [Collas et al., 2015]. However, it was not the same patient.

Met opmaak: Nederlands (België)

Met opmaak: Nederlands (België)

Met opmaak: Nederlands (België)

Image analysis

To extract the patient specific geometries, segmentation of the aortic root was performed on the pre-operative scans using Mimics 16.0 (Materialise N.V., Leuven, Belgium). The left ventricle and aorta were extracted from the CT images using a threshold on the contrast agent in the blood, as depicted in panel A of figure 1. The left ventricle and aorta were separated from connected structures and each other using a graph cut algorithm [Boykov and Kolmogorov, 2004]. 3-dimensional (3D) triangulated parts were created using a marching cubes triangulation (figure 1B). Smoothing was performed to remove noise and small substructures. Three leaflets were created

starting from the result of the graph cut by smoothing and disconnecting the valve surface from the left ventricle. Finally, the calcifications were extracted using a threshold above the intensity of the contrast agent and a region grow in the aortic root, followed by a marching cubes triangulation to generate a triangulated surface.

Based on the 3D triangulated surfaces, a finite element mesh was generated using 3-matic 8.0 (Materialise N.V., Leuven, Belgium). Triangular shell elements were used to model the aortic root and the leaflets (figure 1C). Four node linear tetrahedral elements were used to model the calcifications.

Constitutive material model

An isotropic Neo-Hookean material model was used to model the soft tissues (the aorta, the leaflets, the aortic annulus, the myocardium and the septum between the left ventricle and left atrium). The strain energy density function (ψ), relating stress (σ) to strain (ε) through $\sigma = \frac{\partial \psi}{\partial \varepsilon}$, can be written as:

$$\psi = \frac{\mu}{2}(\bar{I}_1 - 3) + \frac{\kappa}{2}(J-1)^2$$

where μ and κ are the shear modulus and bulk modulus associated with the deviatoric part and the volumetric part respectively of the strain energy density. $\bar{I}_1$ is the first invariant of the deviatoric part of the right Cauchy-Green tensor $\bar{C} = \bar{F}^T\bar{F}$: $\bar{I}_1 = J^{-2/3} I_1$, and J is the determinant of the deformation gradient or Jacobian $J = \det F$. The materials are considered to be nearly incompressible, κ is set to 10 MPa as a compromise between incompressibility and simulation stability [Famaey et al., 2012]. The initial value of μ is chosen based on previous experience in modeling cardiovascular tissue, and subsequently optimized to reach a good correspondence between the final simulation result and the stent extracted from the post-operative CT. Table 1 shows the values of the material parameters and the thickness of the different soft tissues, the density is set to 1000 kg/m^3. The calcifications were modelled using a linear-elastic material with Young's modulus, E = 5 MPa, Possion's coefficient, ν = 0.475 and density, ρ = 1200 kg/m^3, comparable values are found in literature [Holzapfel et al., 2004; Morganti et al., 2014].

Stent model

A µCT scan of the stent in its unloaded state, was made. The scan had a spatial resolution of 59 µm. The centerline of the metal stent struts was computed using Mimics 16.0 (Materialise N.V., Leuven, Belgium). A finite element model, consisting of quadratic beam elements was created, based on the centerline curves. The beam elements had a rectangular cross section (0.15 mm x 0.4 mm). The stent was modelled with a super-elastic Nitinol material model, available in Abaqus [Auricchio and Taylor, 1997; Auricchio et al., 1997]. The parameters for this model are presented in table 2. The density of Nitinol was set to 6450 kg/m^3.

Boundary conditions and simulation set-up

The stent's axial position was based on the depth measured with respect to each of the three leaflets on the post-operative CT scan (figure 1E). This allows for a fair comparison between the simulated geometry and the post-operative geometry of the stent.

The displacement and rotation of the top and bottom nodes of the aortic root were set to zero. The stent diameter was reduced to 10 mm in an offline simulation, resulting in internal stresses in the stent struts which will push open the valve. In the first step, a small pressure was applied to the tip of the leaflets to open the valve, while holding the stent in place by preventing displacement of its nodes. In the second step, general, frictionless contact was applied and the top nodes of the stent were moved down to expand the stent in a controlled way. In this step, contact was made between the stent and the calcified leaflets. In the final step, all boundary conditions on the stent were removed except the z-displacement of the bottom nodes. This allowed for the stent and the aortic root to find an equilibrium configuration.

The simulations for all ten cases were performed using Abaqus 6.13 explicit (SIMULIA, Providence, RI, USA). A mass-scaling of 5 was applied to increase the step time which was automatically optimized by the solver. A quasi-static solution was approached by setting the total step time to 0.55 seconds. Thereby, the resulting kinetic energy in the model was below 5% of the internal energy.

Sensitivity to material model and wall thickness

Only the overall geometry of the aortic root could be derived from the CT scans. Therefore, there were no patient-specific values for the material parameters and the wall thickness. In order to test the sensitivity of the model to those parameters, the shear modulus of all soft tissue elements and the thickness of all shell elements except the leaflets were doubled and halved separately. In addition, all patients were simulated using an anisotropic linear-elastic material for the soft tissue elements. Table 3 contains the material parameters of this model. The circumferential stiffness was chosen to approximate the hyperelastic material properties of the baseline simulation. The longitudinal stiffness is half the circumferential stiffness.

Validation using a post-operative CT scan

The deformed stent geometry was extracted from the post-operative CT using Mimics 16.0 (Materialise N.V., Leuven, Belgium). The Metallic stent was segmented using a high threshold, 1000 Hounsfield units, and region grow of the connected voxels (figure 2L). To extract the calcifications from the post-op CT, a threshold of 600 Hounsfield units was used in combination with a region grow algorithm. By performing a marching cubes algorithm on both masks, this results in two triangulated surfaces. The first surface only contains the stent, it was used to measure the diameter of the device at 4 cross sections, as depicted in figure 2R. The second surface contains the stent and the surrounding calcifications it is depicted in figure 3 overlaid with the simulation results in order to get a qualitative comparison of the result.

To quantify the difference between the simulation result and the post-operative stent geometry, a circle is fitted through the stent struts in 4 cross sections, two at the bottom of the device, one at the narrowest section, where the new valve is situated, and one at top. This is done for both the stent segmented from the post-operative CT scan and the stent geometry in the simulation result.

Aortic regurgitation estimation

Considering the importance of AR, a method was developed to predict the amount of AR based on the simulation result. A shrink-wrap was performed on the simulated stent, using 3-matic 10.0 (Materialise N.V., Belgium), to model the sealing skirt of the CoreValve device. From the nodes of this triangulated surface, the distance to the closest point of the aortic root was calculated (figure 4B). Then, a max-flow algorithm [Boykov and Kolmogorov, 2004] was used to calculate the flow paths from the top edge to the bottom edge of the sealing skirt. The max-flow algorithm takes a 1 dimensional connected graph, representing the flow network, as input. The edges of the triangulated surface, forming the sealing skirt, were used to construct the graph. Each edge forming a connection in the graph has a value representing its flow capacity. This was calculated as the average distance of the edge to the aortic root. Edges with an average distance smaller than 0.5 mm are considered to be in contact with the aortic root. Therefore, their capacity is set to zero.

Results

Table 4 contains the diameter measurements of the post-operative stent geometry derived from the post-operative CT scans. Comparing the diameter with the nominal, fully expanded, diameter shows that the stents have on average the potential to expand another 15% at the bottom, 10% at the narrowest section and 30% at the top in order to reach the nominal stent configuration. In addition, the root mean square (RMS) difference between 3 consecutive measurements on the stents are also presented in table 4. Because the struts of the stents are metal which has a high X-ray absorption compared to the surrounding tissue, the stent model derived from the post-operative CT appears thicker than it is in reality. Therefore, depending on which cross sectional points of the struts are used to calculate the best fit diameter, the results vary. The RMS difference between the measurements gives an idea of the measurement error on the post-operative stent diameter.

Figure 3 depicts an overlay of the simulated stent geometry and the segmented stent and calcifications from the post-operative CT scans. Excluding local deviations, at the bottom of the

device, a good qualitative correspondence between the simulation results and the post-operative stent can be observed for all patients.

Comparing the cross sectional diameters, as depicted in figure 2, of the simulated stent and the post-operative stent, the diameter at section A was underestimated, on average, by 1.1 ± 0.7 mm. The diameter at section B was, on average, slightly underestimated, by 0.2 ± 0.7 mm. The diameter at narrowest section of the stent, section C, was overestimated, on average, by 0.9 ± 0.5 mm. Finally, the diameter of the widest section of the stent, section D, was, on average, very slightly underestimated, by 0.1 ± 1.3 mm. Table 5 contains the average diameter of the baseline simulations and the average difference with the post-operative diameter.

Sensitivity analysis

Table 6 contains the average diameter of the stent for all sensitivity experiments, for each section. In addition, the average difference compared to the baseline simulation is also shown. The largest difference was observed in the experiment where the thickness of the aortic root wall was doubled. The diameter decreased by 6% in section A and section B.

Aortic regurgitation estimation

The results of the leakage estimation are presented in table 7, together with both clinically observed AR grades. Patients 4, 8 and 10 which consistently have no AR in both clinical observations, also have very low maxi-flow values. Patient 7 has the highest max-flow value and also has the higher AR grade immediately after implantation. However, at the second evaluation using echocardiography, patient 9 has the highest AR grade, while the max-flow analysis of that patient resulted in the lowest value excluding the patients without AR.

Discussion

In this paper, a finite element based method was developed to simulate a transcatheter aortic valve implantation in a patient-specific geometry based on pre-operative CT scans. This method was

validated using post-operative CT scans of the implanted device and the surrounding anatomy. The sensitivity to the material parameters and the aortic root thickness, which cannot be determined from the pre-operative CT scan, was tested. In addition, the leakage alongside the implant was estimated based on the simulation result and compared with two clinical evaluations. The described method can form the basis for a pre-interventional planning tool which would provide the clinician with additional information about the best size, type and position of the device prior to the implantation. This could help reduce the incidence of life-limiting post-interventional aortic regurgitation.

In recent literature, several other patient specific finite element modeling strategies for TAVI have been described. The majority discusses a balloon expandable device [Auricchio et al., 2014; Bailey et al., 2015; Capelli et al., 2012; Morganti et al., 2014; Wang et al., 2015, 2012]. Russ *et al.* (2013) perform TAVI simulations with a self-expandable device on the geometry of one patient. They compare the simulation results with the circumference of the post-operative stent, extracted from a CT scan. Comparing rigid, linear-elastic and hyperelastic material models, they find that the hyperelastic material model is most accurate, however the difference with the linear-elastic model is small.

In our study, a large part of the stent expansion occurs without contact to the aortic root, except for the calcified leaflets. Therefore, a large part of the total diameter is due to this free expansion. However, the final shape of the stent varies significantly between patients and adapts to the shape of the aortic root of the patient, as can be seen in figure 3. When comparing the post-operative stents to the full size expanded device, it still has the potential to expand at least 15%, this is probably a result of the oversizing of the device which is routinely performed to reduce the occurrence and severity of paravalvular aortic regurgitation [Holmes et al., 2012; Piazza et al., 2008].

The maximal deviation from the baseline simulation was -6%, it occurred in the two bottom sections after a doubling of the shell thickness. A shell of half the thickness only resulted in an additional

expansion of 3%, this difference shows the nonlinear behavior of the system. All other deviations were around or below 4%, especially the top section showed little sensitivity to any of the parameters, considering its potential to expand further. Therefore, the shape of the aortic root, leaflets and calcifications appears to be the main influence of the shape of the device. This is beneficial for the usability of the method in clinical practice, since the shape of the aortic root and calcifications can be determined patient-specifically from the pre-operative CT scan. Further investigation into the contribution of the calcifications and leaflets is needed to support this observation.

To simulate the behavior of arterial tissue more accurately, an anisotropic hyperelastic representation, such as the Holzapfel-Gasser-Ogden model could have been used [Gasser et al., 2006; Holzapfel et al., 2000]. Wang *et al.* (2015, 2012) used this type of material model in their TAVI models. However, this material model requires an estimation of the collagen fiber orientation and the pre-stress in the aortic root and leaflets. These parameters are very hard to estimate with non-invasive measurements for each patient [Smoljkic et al., 2015]. In this study, the impact of anisotropy was tested using an anisotropic linear-elastic material model with a circumferential stiffness twice as large as the longitudinal stiffness. The sensitivity analysis showed the diameter of the simulated stent didn't differ more than 4.2% on average.

A potential limitation of the model is the absence of a damage mechanism. Prior to the implantation of the device, a balloon expansion of the calcified valve is performed to facilitate the expansion of the actual implant. This was simulated in the model by splitting calcifications which cross leaflet boundaries. In addition, the myocardium is modelled as a passive structure, while in reality it is a muscle with an active component to its compliance.

The position of the implant, used as an input in the simulation, could only be derived from the post-operative CT scan. This violates the strict separation between input and validation data. However, the position of the implant is not part of the evaluation.

In all simulations, the diameter at the narrowest cross section of the stent is larger than the post-operative situation. The cause of this systematic error is currently unknown to us. Therefore, further investigation into the stent model and material parameters is needed.

Comparing the output of the regurgitation estimation, the results were mixed. When both the grades immediately after implantation and at hospital discharge were zero, the results of the analysis corresponded well. However, the patient with problematic AR (grade ≥ 2) is different in the two evaluations. The patient with the highest regurgitation estimate also has the highest grade in the angiographic evaluation immediately after implantation. However, the echocardiographic evaluation at hospital discharge has been proven to be a better predictor of increased mortality [Collas et al., 2015]. The difference between both AR evaluations could be due to the difference in time, the imaging technique or the grading system. True AR volume quantification would be best to evaluate and validate the regurgitation estimation. However, such a measurement is difficult to obtain and was not available for the patients in this study. Further investigation, analyzing more case and other methods, such as computational fluid dynamics, is necessary to determine whether paravalvular AR can be estimated based on the simulation results.

In summary, the results of the simulation show good correspondence with the post-operative outcome of the transcatheter aortic valve implantation, both visually and quantitatively. However, a systematic overestimation of the diameter at the narrowest section of the stent and an underestimation at the bottom can still be observed, both in the order of 1 mm. In addition, low sensitivity of the diameter to the non-patient-specific parameters, wall thickness and material properties, could be observed. The estimation of leakage risk based on the distance between the sealing skirt of the simulated device and the surrounding aortic root, shows promise, especially in the detection of very good implantations. Further research in both the simulation and regurgitation estimation is needed, including more cases, to confirm these results and improve the accuracy. Volume measurements of the aortic regurgitation would be useful to develop and validate the best

approach to predict the aortic regurgitation risk. To conclude, these tools have the potential to help reduce the occurrence of aortic regurgitation in the patient population by providing information on optimal position, type and size of the device for a patient prior to the operation, by virtually testing these different options and evaluating the risk of leakage of every option.

Acknowledgements

This work was supported in part by a PhD grant from the *agency for innovation through science and technology (IWT)* of the Flemish government and in part by the Research Foundation Flanders (FWO).

Conflicts of interest

Prof. Dr. Johan Bosmans is part-time clinical proctor for Medtronic. The remaining authors have no conflicts of interest to declare.

References

Auricchio, F., Conti, M., Morganti, S., Reali, a, 2014. Simulation of transcatheter aortic valve implantation: a patient-specific finite element approach. Comput. Methods Biomech. Biomed. Engin. 17, 1347–57.

Auricchio, F., Taylor, R.L., 1997. Shape-memory alloys : modelling and numerical simulations the finite-strain superelastic behavior. Comput. Methods Appl. Mech. Eng. 7825, 175–194.

Auricchio, F., Taylor, R.L., Lubliner, J., 1997. Shape-memory alloys : macromodelling and numerical simulations of the superelastic behavior. Comput. Methods Appl. Mech. Eng. 7825.

Bailey, J., Curzen, N., Bressloff, N.W., 2015. Assessing the impact of including leaflets in the simulation of TAVI deployment into a patient-specific aortic root. Comput. Methods Biomech. Biomed. Engin. 5842, 1–12.

Bose, A.K., Aitchison, J.D., Dark, J.H., 2007. Aortic valve replacement in octogenarians. J. Cardiothorac. Surg. 2, 33–5.

Boykov, Y., Kolmogorov, V., 2004. An experimental comparison of min-cut/max-flow algorithms for energy minimization in vision. IEEE Trans. Pattern Anal. Mach. Intell. 26, 1124–37.

Capelli, C., Bosi, G.M., Cerri, E., Nordmeyer, J., Odenwald, T., Bonhoeffer, P., Migliavacca, F., Taylor, A.M., Schievano, S., 2012. Patient-specific simulations of transcatheter aortic valve stent implantation. Med. Biol. Eng. Comput. 50, 183–92.

Collas, V.M., Paelinck, B.P., Rodrigus, I.E., Vrints, C.J., Bosmans, J.M., 2015. Aortic regurgitation after transcatheter aortic valve implantation (TAVI) — Angiographic, echocardiographic and hemodynamic assessment in relation to one year outcome. Int. J. Cardiol. 194, 13–20.

Famaey, N., Sommer, G., Vander Sloten, J., Holzapfel, G. a, 2012. Arterial clamping: finite element simulation and in vivo validation. J. Mech. Behav. Biomed. Mater. 12, 107–18.

Met opmaak: Engels (V.S.)

Gasser, T.C., Ogden, R.W., Holzapfel, G. a., 2006. Hyperelastic modelling of arterial layers with distributed collagen fibre orientations. J. R. Soc. Interface 3, 15–35.

Holmes, D.R., Mack, M.J., Kaul, S., Agnihotri, A., Alexander, K.P., Bailey, S.R., Calhoon, J.H., Carabello, B.A., Desai, M.Y., Edwards, F.H., Francis, G.S., Gardner, T.J., Kappetein, A.P., Linderbaum, J.A., Mukherjee, C., Mukherjee, D., Otto, C.M., Ruiz, C.E., Sacco, R.L., Smith, D., Thomas, J.D., 2012. 2012 ACCF/AATS/SCAI/STS Expert Consensus Document on Transcatheter Aortic Valve Replacement. J. Am. Coll. Cardiol. 59, 1200–1254.

Holzapfel, G. a., Sommer, G., Regitnig, P., 2004. Anisotropic Mechanical Properties of Tissue Components in Human Atherosclerotic Plaques. J. Biomech. Eng. 126, 657.

Holzapfel, G.A., Gasser, T.C., Ogden, R.W., 2000. A new constitutive framework for arterial wall mechanics and a comparative study of material models. J. Elast. 61, 1–48.

Kodali, S.K., Williams, M.R., Smith, C.R., Svensson, L.G., Webb, J.G., Makkar, R.R., Fontana, G.P., Dewey, T.M., Thourani, V.H., Pichard, A.D., Fischbein, M., Szeto, W.Y., Lim, S., Greason, K.L., Teirstein, P.S., Malaisrie, S.C., Douglas, P.S., Hahn, R.T., Whisenant, B., Zajarias, A., Wang, D., Akin, J.J., Anderson, W.N., Leon, M.B., 2012. Two-year outcomes after transcatheter or surgical aortic-valve replacement. N. Engl. J. Med. 366, 1686–95.

Leon, M.B., Smith, C.R., Mack, M., Mille, C.D., Moses, J.W., Svensson, L.G., Tuzcu, E.M., Webb, J.G., Fontana, G.P., Makkar, R.R., Brown, D.L., Block, P.C., Guyton, R.A., Pichard, A.D., Bavaria, J.E., Herrmann, H.C., Douglas., P.S., Petersen, J.L., Akin, J.J., Anderson, W.N., Wang, D., Pocock, S., 2010. Transcatheter Aortic-Valve Implantation for Aortic Stenosis in Patients Who Cannot Undergo Surgery. N. Engl. J. Med. 363, 1597–1607.

Linke, A., Wenaweser, P., Gerckens, U., Tamburino, C., Bosmans, J., Bleiziffer, S., Blackman, D., Schafer, U., Muller, R., Sievert, H., Sondergaard, L., Klugmann, S., Hoffmann, R., Tchetche, D., Colombo, A., Legrand, V.M., Bedogni, F., lePrince, P., Schuler, G., Mazzitelli, D., Eftychiou, C.,

Met opmaak: Engels (V.S.)

Frerker, C., Boekstegers, P., Windecker, S., Mohr, F.-W., Woitek, F., Lange, R., Bauernschmitt, R., Brecker, S., 2014. Treatment of aortic stenosis with a self-expanding transcatheter valve: the International Multi-centre ADVANCE Study. Eur. Heart J. 35, 2672–2684.

Morganti, S., Conti, M., Aiello, M., Valentini, a, Mazzola, a, Reali, a, Auricchio, F., 2014. Simulation of transcatheter aortic valve implantation through patient-specific finite element analysis: Two clinical cases. J. Biomech. 47, 2547–2555.

Piazza, N., de Jaegere, P., Schultz, C., Becker, A.E., Serruys, P.W., Anderson, R.H., 2008. Anatomy of the Aortic Valvar Complex and Its Implications for Transcatheter Implantation of the Aortic Valve. Circ. Cardiovasc. Interv. 1, 74–81.

Russ, C., Hopf, R., Hirsch, S., Sundermann, S., Falk, V., Szekely, G., Gessat, M., 2013. Simulation of transcatheter aortic valve implantation under consideration of leaflet calcification. Conf. Proc. IEEE Eng. Med. Biol. Soc. 711–4.

Sellers, R.D., Levy, M.J., Amplatz, K., Lillehei, C.W., 1964. Left retrograde cardioangiography in acquired cardiac disease: Technique, indications and interpretations in 700 Cases. Am. J. Cardiol. 14, 437–447.

Simulia, 2010. Abaqus Technology Brief: Simulation of Implantable Nitinol Stents.

Smoljkic, M., Vander Sloten, J., Segers, P., Famaey, N., 2015. Non-Invasive, enery-based assessment of patient-specific material properties of arterial tissue. Biomech. Model. Mechanobiol.

Thourani, V.H., Ailawadi, G., Szeto, W.Y., Dewey, T.M., Guyton, R. a, Mack, M.J., Kron, I.L., Kilgo, P., Bavaria, J.E., 2011. Outcomes of surgical aortic valve replacement in high-risk patients: a multiinstitutional study. Ann. Thorac. Surg. 91, 49–55; discussion 55–6.

Wang, Q., Kodali, S., Primiano, C., Sun, W., 2015. Simulations of transcatheter aortic valve implantation: implications for aortic root rupture. Biomech. Model. Mechanobiol. 14, 29–38.

Met opmaak: Engels (V.S.)

Wang, Q., Sirois, E., Sun, W., 2012. Patient-specific modeling of biomechanical interaction in transcatheter aortic valve deployment. J. Biomech. 45, 1965–71.

Tables

Table 1: The shear modulus (μ) and thickness (t) of the aorta, annulus, leaflets, septum and myocardium used in the baseline simulation

	μ [KPa]	t [mm]
Aorta	500	1.5
Annulus	200	1
Leaflets	1000	0.5
Septum	100	1
Myocardium	500	5

Table 2: The material parameters of the nitinol stent, for the Abaqus super-elastic nitinol material model [Simulia, 2010]

	E_a [GPa]	ν_a	E_m [GPa]	ν_m	ε^l	$\left(\frac{\delta\sigma}{\delta T}\right)_l$	σ_L^S [MPa]	σ_L^E [MPa]	T_0	$\left(\frac{\delta\sigma}{\delta T}\right)_u$	σ_U^S [MPa]	σ_U^E [MPa]	σ_{CL}^S [MPa]	ε_V^L
Stent	50	0.33	25	0.33	0.07	6.7	380	400	37	6.7	250	220	900	0.07

Table 3: The circumferential (E_c), axial (E_a) and radial (E_r) Young's modulus of the aorta, annulus, septum and myocardium, for the simulation with an anisotropic linear-elastic material model. In addition, the shear modulus (μ) and Poisson's coëfficient (ν) are also shown.

	E_c [KPa]	E_a [KPa]	E_r [KPa]	μ [KPa]	ν
Aorta	850	425	200	200	0.475
Annulus	340	170	85	85	0.475
Septum	170	85	42.5	42.5	0.475
Myocardium	850	425	200	200	0.475

Table 4: The average cross sectional diameter of the post-operative stents and an estimation of the measurement variability

	Section A	Section B	Section C	Section D
Average post-op diameter [mm] (% from full expansion)	25.1 ± 0.9 (15.6%)	24.7 ± 0.6 (17.8%)	21.5 ± 0.6 (11.7%)	31.2 ± 1.5 (38.3%)
RMS difference on diameter measurement [mm]	0.45	0.25	0.21	0.30

RMS = root mean square

Table 5: The average cross sectional diameter of the simulated deployed stent

	Section A	Section B	Section C	Section D
Baseline simulation average diameter [mm] (% from post-op)	23.9 ± 0.8 (-5%)	24.3 ± 0.7 (-1.4%)	22.6 ± 0.4 (5.1%)	31.3 ± 1.5 (0.3%)

Table 6: The average difference from the post-operative stent diameter and the results of the sensitivity simulations

	Section A	Section B	Section C	Section D
2*shear modulus simulation average diameter [mm] (% from Baseline)	23 ± 1.2 (-3.7%)	23.4 ± 1.0 (-3.9%)	22 ± 0.7 (-2.8%)	30.8 ± 1.6 (-1.7%)
½*shear modulus simulation average diameter [mm] (% from Baseline)	24.4 ± 0.7 (2.3%)	24.9 ± 0.6 (2.5%)	23.1 ± 0.4 (2.7%)	31.8 ± 1.7 (1.6%)
Anisotropic simulation average diameter [mm] (% from Baseline)	24.8 ± 0.7 (4.0%)	25.3 ± 0.6 (4.2%)	23.4 ± 0.3 (3.5%)	32.0 ± 1.6 (2.9%)
2*Wall thickness simulation average diameter [mm] (% from Baseline)	22.4 ± 1.3 (-6.3%)	22.9 ± 1.1 (-5.9%)	22.2 ± 0.6 (-2.1%)	30.7 ± 1.7 (-1.8%)
½* Wall thickness simulation average diameter [mm] (% from Baseline)	24.7 ± 0.7 (3.4%)	25.1 ± 0.6 (3.4%)	23.2 ± 0.4 (2.7%)	32.3 ± 1.6 (3.1%)

Table 7: The max-flow analysis on the closest point distance maps of the sealing zone of the simulated stent, in combination with two post-operative aortic regurgitation evaluations

	Max-flow [mm]	Post-op Angiographic AR grade [0 – 4]	7 days post-op Echocardiographic AR grade [0 – 4]
Patient 1	72	0	1
Patient 2	30.3	1	1
Patient 3	56.4	0	1
Patient 4	0	0	0
Patient 5	75.4	1	1
Patient 6	36.1	1	1
Patient 7	138.6	2	1
Patient 8	1.6	0	0
Patient 9	22.5	1	3
Patient 10	7.3	0	0

AR = Aortic Regurgitation

Figures

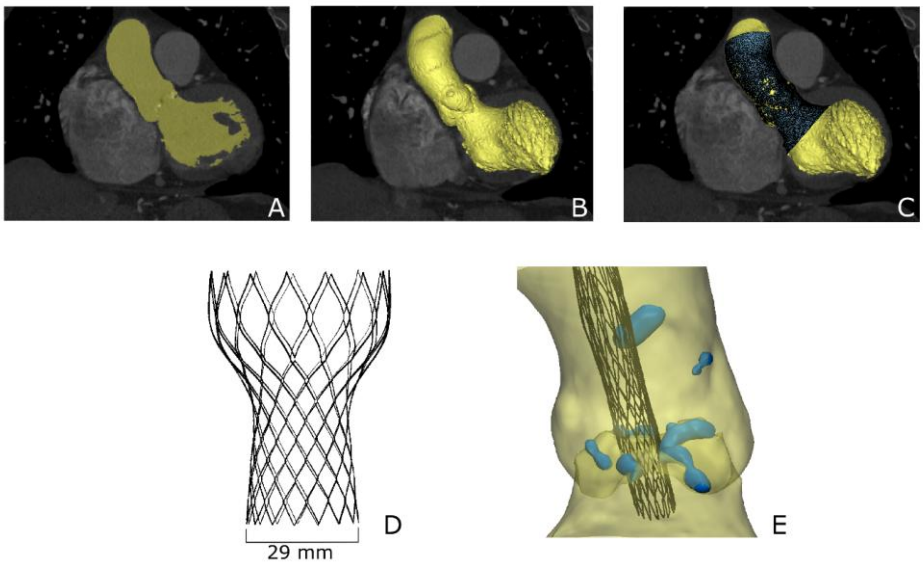

Figure 1: (A) Coronal view of the computed tomography scan of patient 5 with the left chambers and aorta blood pool colored yellow. (B) Three dimensional reconstruction of the relevant geometry. (C) The resulting aortic root model used for finite element simulation. (D) The beam element model of the 29mm CoreValve stent. (E) Positioning of the crimped stent in the calcified aortic root at the start of the simulation

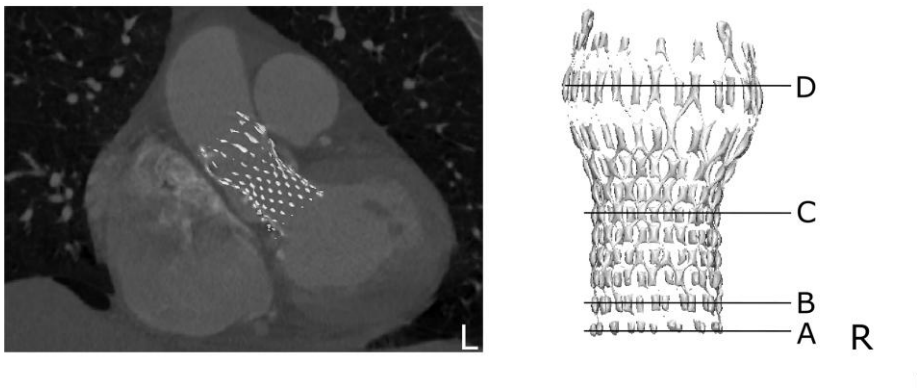

Figure 2: (L) A coronal view of the post-operative computed tomography scan of patient 5 with the segmented stent. (R) An overview of the locations of the cross section diameter measurements

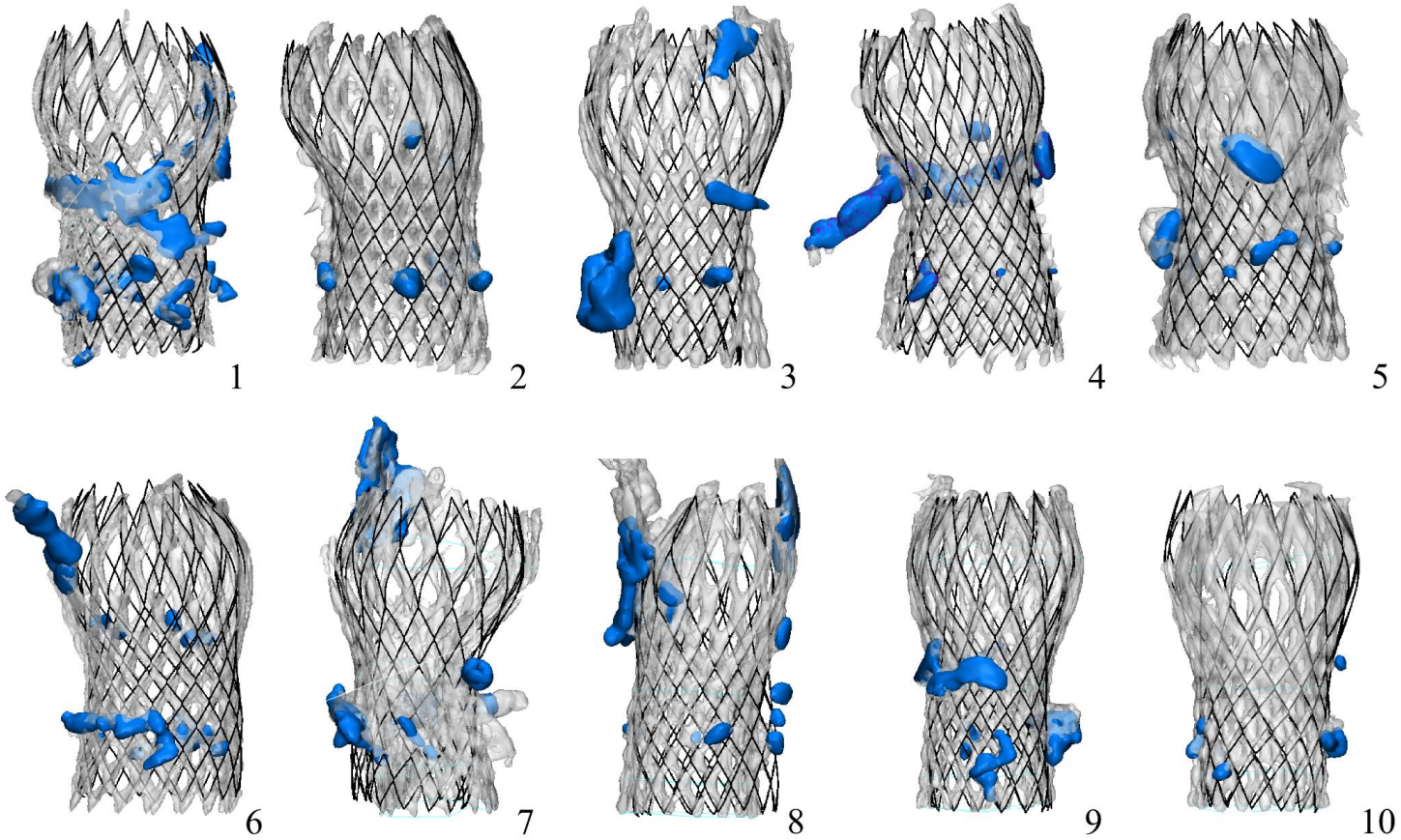

Figure 3: Overview of the simulated deployed stent (black) and calcifications (blue) on top of the post-operative stent and calcifications (white) segmented from the post-operative computed tomography scans

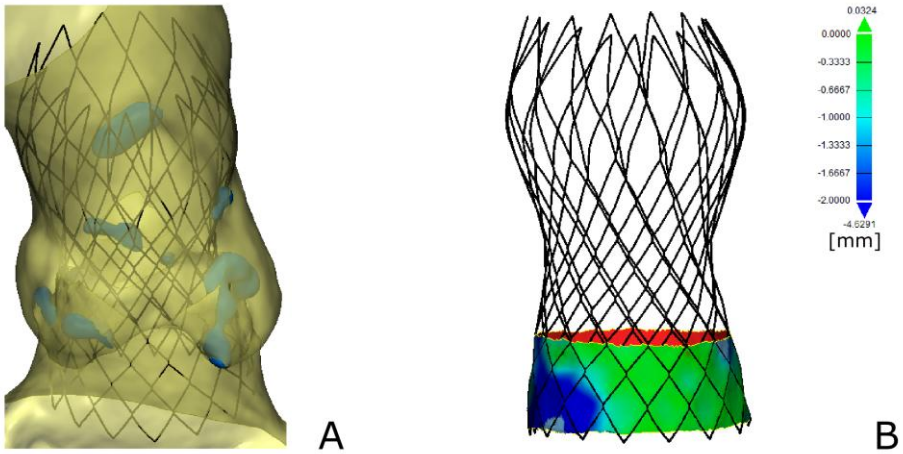

Figure 4: (A) The simulated stent deployed in the calcified aortic root of patient 5. (B) A color map of the closest point distance of the sealing zone to the calcified aortic root